Ice plate deformation and cracking revealed by an *in situ* distributed acoustic sensing array

Jun Xie[1], Xiangfang Zeng[1], Chao Liang[2], Sidao Ni[1], Risheng Chu[1], Feng Bao[1], Rongbing Lin[1], Benxin Chi[1], Hao Lv[1]

[1] State Key Laboratory of Geodesy and Earth's Dynamics, Innovation Academy for Precision Measurement Science and Technology, Chinese Academy of Sciences, Wuhan, 430077, China

[2] Institute for Disaster Management and Reconstruction (IDMR), Sichuan University, Chengdu, 610100, China

Correspondence to: Xiangfang Zeng (zengxf@whigg.ac.cn)

Abstract. Studying seismic sources and wave propagation in ice plates can provide valuable insights into understanding various processes such as ice structure dynamics, migration, fracture mechanics, mass balance, etc. However, the harsh environment makes it difficult to conduct in-situ dense seismic observations. Consequently, our understanding of the dynamic changes within the ice sheet remains insufficient. We conducted a seismic experiment using a distributed acoustic sensing (DAS) array on a frozen lake, exciting water vibrations through underwater airgun shots. By employing an artificial intelligence method, we were able to detect seismic events that includes both high frequency icequakes and low frequency events. The icequakes clustered along ice fractures and its activity correlated with local temperature variations. The waveforms of low frequency events exhibit characteristics of flexural-gravity waves which offers insights into the properties of ice plate. Our study demonstrates the effectiveness of an DAS array as an in-situ dense seismic network for investigating the internal failure process and dynamic deformation of ice plates such as ice shelf, which may contribute to an enhanced comprehension and prediction of ice shelf disintegrations.

1 Introduction

Cryo-seismology, thanks to its high temporal resolution capabilities, has attracted the attention of scientists in the fields of seismology, cryosphere, and climatology. It is regarded as an effective approach for studying glacier dynamics and understanding complex intricate processes (Aster and Winberry, 2017; Podolskiy and Walter, 2016). Seismological records of the cryosphere can be utilized to study the dynamic process occurring on the surface or within glaciers, aiding in the identification of the ice shelf damage, environmental changes and so on. Large glacial earthquakes can be detected by global seismic networks (e.g., Global Seismographic Network), and their mechanisms have been extensively studied, which were associated with iceberg calving and capsizing (Ekström et al., 2003; Sergeant et al., 2019; Veitch and Nettles, 2017). Besides, local microseismicities (such as surface crevasses and basal slip events) can provide more insights into the dynamic change process of glaciers and facilitate the study of glacier disintegration (Helmstetter et al., 2015; Lombardi et al., 2019; Romeyn et al., 2021; Walter et al., 2013). Due to lower released seismic energy and stronger attenuation for higher frequency signal excited by these events, it is crucial to have closely spaced seismic stations (e.g., on the ice surface or in shallow boreholes)

in order to capture signal and analyse the data (Röösli et al., 2014; West et al., 2010). However, the harsh environment and logistical challenges of glaciers make it difficult to deploy dense seismic array for comprehensive long-term monitoring. As a result, researchers even explored the potential of utilizing single seismometer to study icequakes (e.g., Köhler et al., 2019).

35   In recent years, Distributed Acoustic Sensing (DAS) has shown its potential in many applications (Zhan, 2019) such as, microseismic monitoring, seismic imaging, earthquake early warning (e.g., Farghal et al., 2022). DAS arrays have also been deployed in glacier environments. The benefits of their large aperture and dense observation have been demonstrated in the study of glacial structures and the monitoring of icequakes (Booth et al., 2020; Brisbourne et al., 2021; Castongia et al., 2017; Fichtner et al., 2022; Hudson et al., 2021; Walter et al., 2020). Hudson et al. (2021) conducted a study on using DAS to

40   monitor basal icequakes at Rutford Ice Stream. They compared the performance of DAS with a geophone array in terms of icequake detection and location. The study found the DAS is outperformed by the geophone array in monitoring. Their methodology and findings are useful for applying of DAS in glacial environment. Walter et al. (2020) deployed a DAS array in Alpine terrain and they successfully detected glacier stick-slip events which are associated with glacier flow and nearby rock falls. Their work demonstrated the significant potential of DAS for monitoring of glacier dynamics and natural hazards

45   in the mountainous regions. These studies demonstrated logistical feasibility of installing large aperture, high-quality DAS array in glacial environments. However, the use of DAS to study the interaction between water and ice on ice shelves has been limited.

In this study, we deployed a DAS array on the Xiliushui Reservoir, a frozen freshwater lake in Gansu Province, China to explore the effectiveness of using DAS for monitoring the cracking and dynamic flexure of the ice plate (Fig. 1).

50   Seismicities have been observed on frozen lakes similar to icequakes in ice shelf (e.g., Dobretsov et al., 2013; Kavanaugh et al., 2018; Ruzhich et al., 2009). Nziengui-Bâ et al. (2022) obtained the thickness and Young's modulus of the ice pack of a lake with DAS records of hammer tests. Fichtner et al. (2022) deployed fiber-optic cable on a frozen lake of a volcano and detected volcanic tremors. In this study, we employed an underwater AirGun Excitation (AGE) to generate water waves and recorded the resulting ice plate vibrations. Using an AI-based method, we successively detected and classified various

55   seismic events, including both icequakes and Low Frequency Events (LFEs). Subsequently, we conducted an analysis of the seismic signals, examining their characteristics, event occurrence rates and locations. One of the key aspects of our analysis involved estimating the Young's modulus of the ice plate by studying the dispersion of flexural-gravity waves excited by LFEs. Finally, we discussed implications of our experiments for understanding the dynamics of ice shelves in natural settings.

60   **2 Experimental setting**

The experimental site for our study was the Zhangye airgun active source platform, located in Xiliushui Reservoir, in Qilian Mountain, Zhangye City, Gansu Province, China (Fig. 1). The average elevation of the Zhangye airgun active source platform is approximately 1900 meters. The water depth of the Xiliushui Reservoir ranges from 45 to 65 meters. The ice

thickness in the reservoir reaches around 0.5 meters during boreal winter. The active airgun source used in this study was positioned at the centre of the lake, submerged at a depth of 15 meters beneath the water surface (Wei et al., 2018). It has been observed that the bubbles generated by the airgun can induce waterbody vibration (de Graaf et al., 2014). The generated waterbody vibrations closely mimic the characteristics of natural ocean waves, enabling realistic and controlled experiments in the study of ice and wave interaction and related phenomena.

In our experiment, a 1.2 km long standard single-mode fiber-optic cable was installed on the surface of the ice. To ensure proper coupling between the fiber-optic cable and the ice surface, we poured water over the fiber-optic cable which, when frozen, formed a solid bond with the ice and effectively coupled the fiber-optic cable to the ice surface. The fiber-optic cable was laid in two circular patterns around the airgun floating platform. The inner circle is about 340 meters long, spanning channels 470 to 645, and the outer circle is nearly 800 meters long, encompassing channels 51-457 (Fig. 1). The interrogator is an Ovlink DAS unit, which measured longitudinal dynamic strain rates of the fiber-optic cable. In this experiment, we employed a gauge length of 2 meters, which refers to the length of the section of the fiber-optic cable used for measurements. The spatial sampling interval was set at 2 meters, and the temporal sampling rate was set at 1000 Hz. The experiment started at 21:00 p.m. on January 6th (Beijing time) and finished at 17:00 p.m. on January 9th. Unfortunately, some instrument failures occurred during the afternoon of January 8th, resulting in an incomplete record between 11:00 p.m. and 13:00 p.m. During the entire duration of the experiment, a total of 65 hours of data, amounting to nearly 600 GB was recorded. Additionally, a CMG-40T three-component short-period seismometer, equipped with a RefTek 130B data logger, was positioned on the shore to capture ground motion. This seismometer recorded data at a sampling rate of 50 Hz, providing complementary information to the DAS records

3 Seismic events

Throughout the experiment, a total of 239 AGEs were conducted. However, due to an instrumental issue, only 223 AGEs were successively recorded. Previous studies indicated that the near-field AGE waveform mainly comprises two components: the main pulse and low-frequency bubble signal (de Graaf et al., 2014). However, our observations with DAS revealed that the near-field AGE signal exhibits a distinct main pulse (Fig. S1 in the supporting information). Additionally, we observed that the similarity among different AGE waveforms was below 20% (Fig. S2 in the supporting information). The main reason for this phenomenon is likely related to the short observation distance between the DAS array and the airgun source. This proximity may have caused the signal recorded by DAS to be clipped, resulting in the absence of a recognizable main pulse.

In addition to the AGE experiments, we also conducted ten hammering experiments to measure the velocity of seismic waves propagating in the ice plate. The hammering signal primarily contained energy above 100 Hz (Fig. S1 in the supporting information). In the hammering signal, a relatively weak P-wave signal can be observed. By analysing the DAS record along a line aligned with the hammering point, we estimated the P-wave velocity in the ice plate to be approximately

3,200 m/s (Fig. S3 in the supporting information). This estimation is consistent with previous research findings. For instance, Ewing et al. (1934) indicated that the P-wave velocity in thick solid ice ranges from 3,432 to 3,698 m/s. Similarly, Wen et al. (1991) reported that the P-wave velocity in thinner ice layers ranges from 2,000 to 3,040 m/s.

Apart from the AGE and hammering signals, our observations revealed two types of passive source signals (Fig. 2). The first type corresponds to icequake that occur within the ice plate and are characterized by a dominant energy at high frequencies ranging from over 10 Hz to 100s Hz (Fig. 2). These signals are associated with longitudinal waves propagating through the ice plate that cause elongation along the fibre direction (Moreau et al., 2020). During the occurrence of some icequakes, the staff also reported hearing cracking sounds, which aligns previous observations reported by Kavanaugh et al. (2018). The other type is characterized by energy primarily in the lower frequency range (1-10 Hz) and has a duration of about 1 second (Fig. 2). Considering its lower frequency signal, we termed them as Low Frequency Event (LFE). They typically emerged after AGEs and exhibit remarkably similar waveforms and moveouts as shown in Fig. S4 in the supporting information.

4 Detection and location

The application of machine learning in seismology has experienced a significant growth in recent years. Machine learning techniques have been primarily focused on earthquake detection and phase-picking, often applied to regional and global earthquake datasets that rely on conventional seismic arrays (Zhu and Beroza, 2019; Zhou et al., 2019; Ross et al., 2018). In this study, we applied a convolutional neural network (CNN) known as You Only Look Once (YOLO, version 5) (Redmon and Farhadi, 2018) to efficiently scan through the DAS dataset for seismic events and categorize into three groups: AGE, LFE and icequake. This CNN is designed for accurate real-time object detection in video files (Redmon and Farhadi, 2018) and has been successfully utilized for micro-seismic event detection in DAS records (Stork et al., 2020). We converted the record sections of DAS dataset to images. To enhance the signal-noise-ratio (SNR), the DAS data are bandpass filtered within the range of 5-50 Hz and normalized based on the maximum amplitude of the entire record section. We assembled 6-second of data from all channels (51-645) into an image, ensuring a 50% overlap to prevent misdetection. We then down sampled the image into a size of 600 by 600 pixels, resulting in each image being approximately 980 KB in size.

To train the AI model, we manually inspected the seismic data from the first 12 hours and labelled 60 AGEs,122 LFEs and 360 icequakes. This labeled dataset was then split this into training, validation, and test sets using a 4:1:1 ratio. Since the AGE catalogue was well-established, it was used to evaluate the performance of the trained model. To accelerate the training process, we utilized a GPU, which reduced the training time to approximately 3 hours. The performance of the model on the test set is depicted in Fig. S5. The confusion rate was found to be low, indicating accurate classification results. For instance, no AGEs were misclassified as icequake. The recall rate is calculated by dividing the number of True Positives (TP) by the total number of actual positives. TP represents the correct prediction, such as detecting icequake as icequake. The recall rates for AGEs, LFEs and icequakes are 100.0%, 100.0%, and 91.0%, respectively, while the precision for the three groups are

73.0%, 93.0%, and 62.8%, respectively. Finally, we applied trained AI model to scan through the rest of the dataset (39,280 images). In total, we detected 14,498 icequakes and 9,391 LFEs.

130   To gain deeper insights into the mechanism of the seismic sources, we located the identified icequakes and LFEs. Here, we utilized an absolute location method based on the neighbourhood algorithm (Sambridge, 1999). We assumed that the propagation velocity of seismic waves in the ice sheet is isotropic, and set it as an inversion parameter. Since the ice plate is thin, we assume the focal depth to be zero. We used the short-time-average through long-time-average (STA/LTA) method (Stevenson, 1976) to pick arrival. The short and long time-windows are set to 0.05 s and 0.25 s for icequakes, and 0.5 s and

135   2.5 s for LFEs, respectively. During the location inversion, the travel-time misfit of each pick is weighted with the maximum amplitude of each waveform. To assess the error of our location setting, we located those 10 hammering events and compared with their ground truth locations. The results showed that the minimum, maximum and average location errors of hammering events are 5 m, 20 m, and 10.2 m, respectively (Fig. S6 in the supporting information). It is important to note that most of the location results exhibited a bias towards the north direction. This systematic deviation of the location results

140   could be attributed to the systematic bias in the position of fiber-optic cable. We conducted a synthetic test using the theoretical travel times. To calculate the theoretical traveltimes, we assumed the DAS cable was shifted southward by 10 meters and added a random error of 0.01 s to each traveltime. The location results deviated northward from the true location (Fig. S7). This illustrated the systematic bias caused by the misalignment of the fiber-optic cable. Overall, the accuracy of the location in this study is acceptable.

145   We detected 14,498 icequakes, exhibiting a clear diurnal cycle (Fig. 2c) and primarily clustered along the promising fractures (Fig. 2d). The number of icequakes does not seem to be associated with AGEs but is rather correlated with the local temperature variation (Fig. 2c). This phenomenon has also been reported by previous studies, for instance, Goto et al. (1980) observed that there was a strong correlation between the occurrence of icequake and the temporal variation of temperature differences within the ice plate. This reveals the nature of icequakes in our experiments as brittle failure of ice plate caused

150   by uneven thermal expansion. The icequake interevent distribution follows a Poisson distribution (Fig. S8 in the supporting information), suggesting that the occurrence of icequake is random, similar to tectonic earthquakes (Rydelek and Sacks, 1989). This implies that there is no specific temporal or spatial pattern governing the occurrence of icequake, and they occur independently of each other. This information is important for understanding the behaviour of icequake and its relationship to other geophysical phenomena. It is worth noting the surge of icequake activity since the noon of January 9th probably

155   indicates a heightened development of cracks within the ice plate. There also seems to be a slight delay between the icequake activity and the temperature, which is probably due to lag from thermal diffusion. A similar delay was reported in Goto et al. (1980), in which the time lag is about 2 hours. In this study, we did not directly measure the ice temperature, but instead relied on the air temperature data. Future work should consider incorporating a combined approach using distributed temperate sensing (DTS) (e.g., Selker et al., 2006) as well as *in situ* DAS observations to establish a more accurate

160   correlation between temperature variation and icequake activity. Besides, a longer observation period in real glacial environments is required to gain a more comprehensive understanding of the relationship.

Among all the detected events, a total of 9,391 were classified as LFEs. These LFEs exhibit a tendency to cluster primarily in the central region of the lake, as well as in close proximity to the airgun floating platform (Fig. 2d). The analysis reveals a close association between LFEs and AGEs, with LFEs generally following AGEs closely in time. However, the

165   detectability of LFEs may vary for different AGEs due to varying noise levels. LFEs are predominantly detected within the first 5 minutes following AGE, but become challenging to observe thereafter (Fig. 2c and further supported by Fig. S9 in the supporting information). In the meantime, the occurrence interval of LFE does not follow the Poisson distribution (Fig. S10 in the supporting information). These observations suggest that there may be a temporal relationship or dependency between AGEs and LFEs, indicating potential interactions or triggering mechanisms between these seismic events and LFEs are

170   likely the waterbody vibrations following the AGEs.

5 Dispersion curve of LFE

Extracting the dispersion relation from the waveforms of LFEs is a valuable approach to gaining deeper understanding of LFE mechanism and signal propagation. Since the LFEs waveforms share a similar moveout patterns (Fig. S4 in the supporting information), we stacked similar waveforms from a series of LFEs to improve SNR. By selecting a master LFE

175   event, we aligned waveforms of other LFEs with time shifts obtained from moving cross-correlation analysis. Stacking aligned waveforms effectively increases the amplitude of the coherent LFE signals while the random noise is reduced. As a quality control, we applied a threshold for the cross-correlation coefficient to retain only the waveforms that well correlated with the master waveform. Specifically, we considered waveforms with a cross-correlation coefficient greater than 0.7 as indicative of a significant correlation. The resulting stacked waveforms, which are shown in Fig. 3, exhibit a clear inverse

180   dispersion pattern. This pattern implies that the LFE signals with higher frequencies arrive earlier than those with lower frequencies.

After obtaining the stacked LFE waveforms, we applied the multi-channel surface wave analysis method developed by Park et al. (1999) to extract the phase velocity dispersion curve. This method allows to analyse the surface wave signals present in the stacked LFE waveforms and determine the variation of phase velocity with respect to frequency. In the

185   frequency range of 1 to 15 Hz, the phase velocity varies from 20 to 160 m/s. This range is significantly lower than the typical shear wave velocity of ice, which is around 1400 m/s as reported by Hudson et al. (2021). This dispersion curve displays the distinctive characteristic of the Flexural-Gravity Wave (FGW) (Williams and Robinson, 1981), which is a special guided wave driven by restoring forces from ice plate flexure and gravity. It corresponds to the Quasi-Scholte mode (QS) seismic wavefield of a thin floating ice plate (Moreau et al., 2020; Nziengui-Bâ et al., 2022).

190   The phase velocity dispersion curve of FGW can be written as (Liu and Mollo-Christensen, 1988),

$$(2\pi f)^2 = \frac{(gk + Dk^5 - Qk^3)}{\coth kH + kM} \tag{1}.$$

where g is the gravity acceleration, k is wavenumber, H is the water depth which is 60 meters in this study, D is the bending modulus, which is a function of ice properties, $D = Eh^3/\rho_w 12(1 - v^2)$, where E is the Young's modulus, υ is the Poisson ratio, h is the ice thickness which is 0.5 meters in this study, ρ_w is the density of water. Q is ice compression, $Q = Ph/\rho_i$, where ρ_i is the density of ice. M is mass loading, $M = h\rho_i/\rho_w$. M and Q are much smaller than gravity and flexural terms and can be neglected (Sutherland and Rabault, 2016). The dispersion equation can be rewritten as,

$$(2\pi f)^2 = \frac{(gk + k^5 Eh^3/\rho_w 12(1 - v^2))}{\coth kH + kM} \tag{2}.$$

The Young's Modulus can also be determined with compressional wave velocity Vp, $E = V_p^2 \rho(1 - v^2)$, assuming v=0.33, according to the results from Fig. S3, E is 9.12 GPa.

The dispersion of the FGW is largely controlled by the ice plate thickness and Young's modulus (Zhao et al., 2018; Sergienko, 2017; Sutherland & Rabault, 2016; Timco & Frederking, 1983; Yang & Yates, 1995). Given a roughly known ice plate thickness (~0.5 m), we successfully explained the observed dispersion curve using the theoretical prediction of FGW (equation 1) with an ice Young's modulus (E) around 10 GPa, which is very close to the one for fresh water ice (Timco & Weeks, 2010). However, Young's modulus and ice thickness are strongly correlated. Thus, a large uncertainty on one of the two parameters will have the same effect on the other. Therefore a joint inversion method combines quasi-Scholte mode and quasi-symmetric mode (corresponds to compressional waves) following a Bayesian scheme should be used to simultaneously invert the thickness and the Young's modulus, and can obtain more accurate results (Nziengui-Bâ et al., 2022). Since the frequency-thickness is much less than 50 Hz·m, the thin plate model (equation 1) is still valid in this study. In other case with thick ice plate, full elastic model (e.g., Mindlin, 1951) could be used.

6 Discussion

The effective modulus of ice reflects its elastic and viscous deformation characteristics, which can be influenced by various factors, including strain rate, temperature, density, ice type, purity and existence of cracks. (Sinha, 1989). Considering the complex nature of ice and its sensitivity to various factors, understanding the effective modulus provides valuable insights into the deformation behaviour and mechanical properties of ice under different conditions. Researchers study these relationships to improve our understanding of ice mechanics and its applications in various fields, such as glaciology, geophysics, and engineering. In the study of Nziengui-Bâ et al. (2022), the Young's Modulus is below 5 GPa. They suspected that this value is underestimated due to snow covering the ice surface or heterogeneity/porosity of the solid columnar ice layer. In the study by Gold (1988), the Young's modulus falls into the range of 4.7-10.4 GPa. Northwood (1947) estimated the Young's modulus of ice to be 9.8 GPa. This value falls within the range reported by Gold (1988) and provides

220 additional support for the Young's Modulus of ice. Another study by Petrovic (2003) reported a slightly wider range for the Young's modulus of ice, between 9.7 and 11.2 GPa.

Deformations caused by ocean waves, such as FGW, play a significant role in the stability of ice shelves and can potentially result in their fragmentation or trigger calving events (Collins III et al., 2015; Liu and Mollo-Christensen, 1988). However, direct observation of the dispersion of the FGW is limited in previous studies (e.g., Sutherland and Rabault, 2016).

225 In this study, we successfully obtained clear records of the FGW. The dispersion of FGW can be used to estimate thickness of the ice plate, which is of significant importance, especially in situations where ice thickness determination is not well resolved, as commonly encountered on ice shelves. Therefore, the accurate recording of FGW on DAS provides a valuable means for inferring both the ice shelf thickness and Young's Modulus. In cracked ice plates, it is commonly observed that the strength usually decreases compared to the individual grains, which is typically around 12 GPa. This suggests that the

230 thickness of the grain boundaries could potentially be estimated using the effective modulus (Wang et al., 2008). Renshaw et al. (2020) also reported that the Young's modulus initially is around 9.5 GPa but starts to decrease once the ice is compressed uniaxially and saturates at about 8.5 GPa along the loading direction and 7 GPa along two other directions perpendicular to the loading direction. In our case, the presence of the AGE resulted in severe fracturing of the ice plate near the AirGun floating platform (Fig. 1). The dispersion curves of FGW for inner circle corroborate our speculation (Fig. S11 in

235 the supporting information), which also provide an explanation for the observed lower phase velocity of FGW around 10 Hz in Fig. 3c. The dispersion curve of FGW obtained from the hammer signal (red triangle in Fig. 1) also reveals a smaller Young's modulus (Fig. S12 in the supporting information). While our experiment was conducted over a 3-day period on a frozen lake spanning a few hundred meters, we acknowledged its limitations in terms of duration and spatial coverage. However, it is possible to monitor the temporal variations in Young's Modulus or thickness of the ice shelf plate with longer

240 continuous observations. Additionally, deploying a longer DAS cable holds the potential to capture the attenuation effect of the ice plate, as highlighted by previous studies (e.g., Yang and Yates, 1995). This would not only enhance our understanding of wave propagation characteristics but also provide valuable insights into the dynamic changes occurring within the ice plate and its response to environmental changes.

Previous studies have shown that FGW has the potential to induce icequakes on ice shelves. The interaction between

245 ocean waves and the ice shelf can lead to dynamic stress and strain variations, which can trigger seismic activities such as icequakes. Studies such as Zhao et al. (2019) have shown that icequakes exhibit spatial and seasonal correlations with ocean gravity waves. This association between icequakes and ocean waves suggests that the interaction between the two can have significant implications for the stability and integrity of ice shelves (Zhao et al., 2019). The energy transferred from the ocean waves to the ice shelf through processes like flexure and wave-induced vibrations can contribute to the fracturing and

250 weakening of the ice, ultimately increasing the risk of ice shelf disintegration. Olinger et al. (2019) found thermal and tidal stresses are important in generating icequakes on the ice shelf. In our experiment, we observed that the number of icequakes did not show a significant change after the AGE (Fig. S13 in the supporting information). This suggests that there may not be a strong correlation between the airgun shot or FGW and the occurrence of icequakes. It is important to note that the

absence of a clear correlation in our experiment does not necessarily rule out the possibility of interactions between icequakes and these external factors in other contexts or under different conditions. We even observed a slight decrease in the number of icequakes after the AGE, which could be attributed to the reduced detection capability caused by strong AGE coda. This discrepancy highlights the potential structural difference between the ice plate on a frozen lake and a real ice shelf. It emphasizes the importance of conducting more on-site seismic observations on real ice shelves to gain a deeper understanding of their dynamics and behaviour. Future studies incorporating comprehensive field observations on actual ice shelves will provide valuable insights into the response and behaviour of icequakes, leading to a better understanding of the factors influencing icequake occurrence and the potential impacts on ice shelf stability. Moreover, DAS array on the seafloor is necessary to monitor the ocean wave and study the response of the ice shelf to the ocean waves (Lindsey et al., 2019).

Our study highlights the potential of DAS in monitoring the formation and progression of ice cracks using passive source signals recorded in similar ice shelf studies. This approach is particularly useful in cases where there is a firn layer on the ice and remote sensing methods are challenging to employ. Furthermore, the variations of FGW can offer valuable information about the heterogeneity of ice plate, which can potentially help infer the size and distribution of the ice plate fragments. It is important to note that our experiment was conducted on an ice-covered lake, and to extend the applicability of these findings to ice shelves, spatial sampling and optimization of the array layout should be considered. For example, by deploying fiber-optic cable spanning hundreds of meters, we can accurately locate icequakes with a precision of meters, and we can also measure longer wavelength FGW. However, measuring FGW induced by ocean wave on ice shelf becomes challenges, since longer wavelength (up to 10 s·km) requires larger aperture array and dominant frequency is down to 0.1 Hz (Zhao et al., 2018). By extending the length of the fiber-optic cable to several kilometres, we can probably capture FGW with larger wavelengths. However, there are other limitations that need to be addressed in future studies, for example, the coupling of fiber-optic cables with the ice on real ice shelves presents a significant challenge in practical applications due to harsh environmental conditions. Moreover, the conventional DAS fibre only measures a single strain component along the cable and does not provide polarization information, which increases the difficulty of identifying seismic phases (Hudson et al., 2021), and the absence of horizontal shear mode introduces additional uncertainty in estimating ice properties (Nziengui-Bâ et al., 2022). One potential remedy to address this is using helically wound fibre (Ning and Sava, 2018).

7 Conclusion

In this study, we analyzed data of a dense DAS array deployed on a frozen lake, which enables the observation of a substantial amount of seismicities associated with ice dynamics. Utilizing a machine learning method, we identified two types of seismic events, namely, icequakes and LFEs. Icequakes exhibited good correlations with ice fractures and local air temperature. The precise location of icequake provided a depiction of ice fracture map. The icequake frequency showed a positive correlation with air temperature, that is, higher temperature results in more icequakes. The LFEs were identified as dynamic flexure of the ice plate. The dispersion curve of LFE signal was used to investigate the Young's modulus of ice,

which is close to 9 GPa in this study. The methods used in this study can be applied to glaciers and ice shelves for monitoring microseismicity and icebody itself. Especially, deploying DAS array with a larger aperture on ice shelf is possible to capture longer-period LFE signal, providing constraints on physical properties such as thickness and Young's modulus of ice shelf. Moreover, DAS based seismic activity observations combined with remote sensing techniques can provide us with more in-depth monitoring and research on dynamic changes and disintegration processes.

Author contributions

XZ planned the campaign; RL performed the measurements; JX, XZ, CL, FB and HL analyzed the data; JX wrote the manuscript draft; JX, XZ, CL, SN, RC, BC and FB reviewed and edited the manuscript.

Code and data availability

The DAS event data is available on https://www.zenodo.org/record/7424310. YOLOv5 can be found https://github.com/ultralytics/yolov5. NA code can be found http://rses.anu.edu.au/~malcolm/na/

Competing interests

The authors declare that they have no conflict of interest.

Acknowledgements

The authors thank Baoshan Wang, Rui Zou, Yahong Wang for their help on the experiment setup and data requisition. We thank Herb Wang (UW-Madison) and Daoyuan Sun (USTC) for their insightful suggestions. The authors thank two anonymous reviewers and editor Petra Heil for their constructive comments.

Financial support

This work was supported by the National Natural Science Foundation of China with grant number 42274076, 42325401 and 42030311, the Youth Innovation Promotion Association of the Chinese Academy of Sciences under grant No. 2022335, and the Foundation for Innovative Research Groups of the Hubei Natural Science Foundation (2023FA040).

References

Aster, R. C. and Winberry, J. P.: Glacial seismology, Rep. Prog. Phys., 80, 126801, https://doi.org/10.1088/1361-6633/aa8473, 2017.

310 Booth, A. D., Christoffersen, P., Schoonman, C., Clarke, A., Hubbard, B., Law, R., Doyle, S. H., Chudley, T. R., and Chalari, A.: Distributed Acoustic Sensing of Seismic Properties in a Borehole Drilled on a Fast-Flowing Greenlandic Outlet Glacier, Geophysical Research Letters, 47, e2020GL088148, https://doi.org/10.1029/2020GL088148, 2020.

Brisbourne, A. M., Kendall, M., Kufner, S.-K., Hudson, T. S., and Smith, A. M.: Downhole distributed acoustic seismic profiling at Skytrain Ice Rise, West Antarctica, The Cryosphere, 15, 3443–3458, https://doi.org/10.5194/tc-15-3443-2021, 315 2021.

Castongia, E., Wang, H. F., Lord, N., Fratta, D., Mondanos, M., and Chalari, A.: An Experimental Investigation of Distributed Acoustic Sensing (DAS) on Lake Ice, JEEG, 22, 167–176, https://doi.org/10.2113/JEEG22.2.167, 2017.

Chen, Z., Bromirski, P. D., Gerstoft, P., Stephen, R. A., Wiens, D. A., Aster, R. C., and Nyblade, A. A.: Ocean-excited plate waves in the Ross and Pine Island Glacier ice shelves, Journal of Glaciology, 64, 730–744, 320 https://doi.org/10.1017/jog.2018.66, 2018.

Chen, Z., Bromirski, P. D., Gerstoft, P., Stephen, R. A., Lee, W. S., Yun, S., Olinger, S. D., Aster, R. C., Wiens, D. A., and Nyblade, A. A.: Ross Ice Shelf Icequakes Associated With Ocean Gravity Wave Activity, Geophysical Research Letters, 46, 8893–8902, https://doi.org/10.1029/2019GL084123, 2019.

Collins III, C. O., Rogers, W. E., Marchenko, A., and Babanin, A. V.: In situ measurements of an energetic wave event in the 325 Arctic marginal ice zone, Geophysical Research Letters, 42, 1863–1870, https://doi.org/10.1002/2015GL063063, 2015.

Dobretsov, N. L., Ruzhich, V. V., Psakhie, S. G., Chernykh, E. N., Shilko, E. V., Levina, E. A., and Ponomareva, E. I.: Advance in earthquake prediction by physical simulation on the baikal ice cover, Phys Mesomech, 16, 52–61, https://doi.org/10.1134/S1029959913010062, 2013.

Ekström, G., Nettles, M., and Abers, G. A.: Glacial Earthquakes, Science, 302, 622–624, 330 https://doi.org/10.1126/science.1088057, 2003.

Ewing, M., Crary, A. P., and Thorne, A. M., Jr.: Propagation of Elastic Waves in Ice. Part I, Physics, 5, 165–168, https://doi.org/10.1063/1.1745245, 2004.

Farghal, N. S., Saunders, J. K., and Parker, G. A.: The Potential of Using Fiber Optic Distributed Acoustic Sensing (DAS) in Earthquake Early Warning Applications, Bulletin of the Seismological Society of America, 112, 1416–1435, 335 https://doi.org/10.1785/0120210214, 2022.

Fichtner, A., Klaasen, S., Thrastarson, S., Çubuk-Sabuncu, Y., Paitz, P., and Jónsdóttir, K.: Fiber-Optic Observation of Volcanic Tremor through Floating Ice Sheet Resonance, The Seismic Record, 2, 148–155, https://doi.org/10.1785/0320220010, 2022.

Gold, L. W.: On the elasticity of ice plates, Can. J. Civ. Eng., 15, 1080–1084, https://doi.org/10.1139/l88-140, 1988.

340 Goto, K., H, H., and Y, W.: A study on ice faulting and icequake activity in the lake Suwa, (3) icequake activity and thermal stresses in ice plate, The science reports of the Tohoku University. Fifth series, Tohoku Geophysical Journal, 1980.

de Graaf, K. L., Brandner, P. A., and Penesis, I.: The pressure field generated by a seismic airgun, Experimental Thermal and Fluid Science, 55, 239–249, https://doi.org/10.1016/j.expthermflusci.2014.02.025, 2014.

Helmstetter, A., Nicolas, B., Comon, P., and Gay, M.: Basal icequakes recorded beneath an Alpine glacier (Glacier
345   d'Argentière, Mont Blanc, France): Evidence for stick-slip motion?, Journal of Geophysical Research: Earth Surface, 120, 379–401, https://doi.org/10.1002/2014JF003288, 2015.

Hudson, T. S., Baird, A. F., Kendall, J. M., Kufner, S. K., Brisbourne, A. M., Smith, A. M., Butcher, A., Chalari, A., and Clarke, A.: Distributed Acoustic Sensing (DAS) for Natural Microseismicity Studies: A Case Study From Antarctica, Journal of Geophysical Research: Solid Earth, 126, e2020JB021493, https://doi.org/10.1029/2020JB021493, 2021.

350 Kavanaugh, J., Schultz, R., Andriashek, L. D., van der Baan, M., Ghofrani, H., Atkinson, G., and Utting, D. J.: A New Year's Day icebreaker: icequakes on lakes in Alberta, Canada, Canadian Journal of Earth Sciences, 56, 183–200, https://doi.org/10.1139/cjes-2018-0196, 2018.

Köhler, A., Maupin, V., Nuth, C., and Pelt, W. van: Characterization of seasonal glacial seismicity from a single-station on-ice record at Holtedahlfonna, Svalbard, Annals of Glaciology, 60, 23–36, https://doi.org/10.1017/aog.2019.15, 2019.

355 Lindsey, N. J., Dawe, T. C., and Ajo-Franklin, J. B.: Illuminating seafloor faults and ocean dynamics with dark fiber distributed acoustic sensing, Science, 366, 1103–1107, https://doi.org/10.1126/science.aay5881, 2019.

Liu, A. K. and Mollo-Christensen, E.: Wave Propagation in a Solid Ice Pack, Journal of Physical Oceanography, 18, 1702–1712, https://doi.org/10.1175/1520-0485(1988)018<1702:WPIASI>2.0.CO;2, 1988.

Lombardi, D., Gorodetskaya, I., Barruol, G., and Camelbeeck, T.: Thermally induced icequakes detected on blue ice areas of
360   the East Antarctic ice sheet, Annals of Glaciology, 60, 45–56, https://doi.org/10.1017/aog.2019.26, 2019.

Mindlin, R. D.: Influence of Rotatory Inertia and Shear on Flexural Motions of Isotropic, Elastic Plates, Journal of Applied Mechanics, 18, 31–38, https://doi.org/10.1115/1.4010217, 1951.

Moreau, L., Boué, P., Serripierri, A., Weiss, J., Hollis, D., Pondaven, I., Vial, B., Garambois, S., Larose, É., Helmstetter, A., Stehly, L., Hillers, G., and Gilbert, O.: Sea Ice Thickness and Elastic Properties From the Analysis of Multimodal Guided
365   Wave Propagation Measured With a Passive Seismic Array, Journal of Geophysical Research: Oceans, 125, e2019JC015709, https://doi.org/10.1029/2019JC015709, 2020.

Ning, I. L. C. and Sava, P.: High-resolution multi-component distributed acoustic sensing, Geophysical Prospecting, 66, 1111–1122, https://doi.org/10.1111/1365-2478.12634, 2018.

Northwood, T. D.: Sonic determination of the elastic properties of ice, Can. J. Res., 25a, 88–95, https://doi.org/10.1139/cjr47a-
370   011, 1947.

Nziengui-Bâ, D., Coutant, O., Moreau, L., and Boué, P.: Measuring the thickness and Young's modulus of the ice pack with DAS, a test case on a frozen mountain lake, Geophysical Journal International, ggac504, https://doi.org/10.1093/gji/ggac504, 2022.

Olinger, S. D., Lipovsky, B. P., Wiens, D. A., Aster, R. C., Bromirski, P. D., Chen, Z., Gerstoft, P., Nyblade, A. A., and Stephen, R. A.: Tidal and Thermal Stresses Drive Seismicity Along a Major Ross Ice Shelf Rift, Geophysical Research Letters, 46, 6644–6652, https://doi.org/10.1029/2019GL082842, 2019.

Park, C. B., Miller, R. D., and Xia, J.: Multimodal analysis of high frequency surface waves, in: Proceedings of the symposium on the application of geophysics to engineering and environmental problems, 00000, 115–121, 1999.

Petrovic, J. J.: Review Mechanical properties of ice and snow, Journal of Materials Science, 38, 1–6, https://doi.org/10.1023/A:1021134128038, 2003.

Podolskiy, E. A. and Walter, F.: Cryoseismology, Reviews of Geophysics, 54, 708–758, https://doi.org/10.1002/2016RG000526, 2016.

Redmon, J. and Farhadi, A.: YOLOv3: An incremental improvement, ArXiv, abs/184.02767, 2018.

Renshaw, C. E., Schulson, E. M., Iliescu, D., and Murzda, A.: Increased Fractured Rock Permeability After Percolation Despite Limited Crack Growth, Journal of Geophysical Research: Solid Earth, 125, e2019JB019240, https://doi.org/10.1029/2019JB019240, 2020.

Romeyn, R., Hanssen, A., Ruud, B. O., Stemland, H. M., and Johansen, T. A.: Passive seismic recording of cryoseisms in Adventdalen, Svalbard, The Cryosphere, 15, 283–302, https://doi.org/10.5194/tc-15-283-2021, 2021.

Röösli, C., Walter, F., Husen, S., Andrews, L. C., Lüthi, M. P., Catania, G. A., and Kissling, E.: Sustained seismic tremors and icequakes detected in the ablation zone of the Greenland ice sheet, Journal of Glaciology, 60, 563–575, https://doi.org/10.3189/2014JoG13J210, 2014.

Ross, Z. E., Meier, M.-A., and Hauksson, E.: P Wave Arrival Picking and First-Motion Polarity Determination With Deep Learning, Journal of Geophysical Research: Solid Earth, 123, 5120–5129, https://doi.org/10.1029/2017JB015251, 2018.

Ruzhich, V. V., Psakhie, S. G., Chernykh, E. N., Bornyakov, S. A., and Granin, N. G.: Deformation and seismic effects in the ice cover of Lake Baikal, Russian Geology and Geophysics, 50, 214–221, https://doi.org/10.1016/j.rgg.2008.08.005, 2009.

Rydelek, P. A. and Sacks, I. S.: Testing the completeness of earthquake catalogues and the hypothesis of self-similarity, Nature, 337, 251–253, https://doi.org/10.1038/337251a0, 1989.

Sambridge, M.: Geophysical inversion with a neighbourhood algorithm—I. Searching a parameter space, Geophysical Journal International, 138, 479–494, https://doi.org/10.1046/j.1365-246X.1999.00876.x, 1999.

Selker, J., van de Giesen, N., Westhoff, M., Luxemburg, W., and Parlange, M. B.: Fiber optics opens window on stream dynamics, Geophysical Research Letters, 33, https://doi.org/10.1029/2006GL027979, 2006.

Sergeant, A., Mangeney, A., Yastrebov, V. A., Walter, F., Montagner, J.-P., Castelnau, O., Stutzmann, E., Bonnet, P., Ralaiarisoa, V. J.-L., Bevan, S., and Luckman, A.: Monitoring Greenland ice sheet buoyancy-driven calving discharge using glacial earthquakes, Annals of Glaciology, 60, 75–95, https://doi.org/10.1017/aog.2019.7, 2019.

Sergienko, O. V.: Behavior of flexural gravity waves on ice shelves: Application to the Ross Ice Shelf, Journal of Geophysical Research: Oceans, 122, 6147–6164, https://doi.org/10.1002/2017JC012947, 2017.

Sinha, N. K.: Elasticity of natural types of polycrystalline ice, Cold Regions Science and Technology, 17, 127–135, https://doi.org/10.1016/S0165-232X(89)80003-5, 1989.

Stevenson, P. R.: Microearthquakes at Flathead Lake, Montana: A study using automatic earthquake processing, The Bulletin of the Seismological Society of America, 66, 61–80, https://doi.org/10.1785/BSSA0660010061, 1976.

Stork, A. L., Baird, A. F., Horne, S. A., Naldrett, G., Lapins, S., Kendall, J.-M., Wookey, J., Verdon, J. P., Clarke, A., and Williams, A.: Application of machine learning to microseismic event detection in distributed acoustic sensing data, GEOPHYSICS, 85, KS149–KS160, https://doi.org/10.1190/geo2019-0774.1, 2020.

Sutherland, G. and Rabault, J.: Observations of wave dispersion and attenuation in landfast ice, Journal of Geophysical Research: Oceans, 121, 1984–1997, https://doi.org/10.1002/2015JC011446, 2016.

Timco, G. W. and Frederking, R. M. W.: Flexural strength and fracture toughness of sea ice, Cold Regions Science and Technology, 8, 35–41, https://doi.org/10.1016/0165-232X(83)90015-0, 1983.

Veitch, S. A. and Nettles, M.: Assessment of glacial-earthquake source parameters, Journal of Glaciology, 63, 867–876, https://doi.org/10.1017/jog.2017.52, 2017.

Walter, F., Dalban Canassy, P., Husen, S., and Clinton, J. F.: Deep icequakes: What happens at the base of Alpine glaciers?, Journal of Geophysical Research: Earth Surface, 118, 1720–1728, https://doi.org/10.1002/jgrf.20124, 2013.

Walter, F., Gräff, D., Lindner, F., Paitz, P., Köpfli, M., Chmiel, M., and Fichtner, A.: Distributed acoustic sensing of microseismic sources and wave propagation in glaciated terrain, Nature Communications, 11, 2436, https://doi.org/10.1038/s41467-020-15824-6, 2020.

Wang, Y., Ballarini, R., and Rodin, G. J.: Crack-Tip Parameters in Polycrystalline Plates with Soft Grain Boundaries, Journal of Engineering Mechanics, 134, 100–109, https://doi.org/10.1061/(ASCE)0733-9399(2008)134:1(100), 2008.

Wei, C., Qin, M., Zhang, Y., Zou, R., Wang, L., Guo, X., Liu, X., Wang, Y., and Sun, D.: Airgun Excitation Experiments at Different Placement Depths in the Qilian Mountain of Gansu Province, China, Seismological Research Letters, 89, 974–982, https://doi.org/10.1785/0220170253, 2018.

Wen, T., Garrison, G. R., Francois, R. E., Stein, R. P., and Felton, W. J.: Sound Speed, Reflectivity, and Absorption Measurements in Arctic Ice in 1988, sound speed reflectivity & absorption measurements in arctic ice in, 1991.

West, M. E., Larsen, C. F., Truffer, M., O'Neel, S., and LeBlanc, L.: Glacier microseismicity, Geology, 38, 319–322, https://doi.org/10.1130/G30606.1, 2010.

Williams, R. T. and Robinson, E. S.: Flexural waves in the Ross Ice Shelf, Journal of Geophysical Research: Oceans, 86, 6643–6648, https://doi.org/10.1029/JC086iC07p06643, 1981.

Yang, T. C. and Yates, T. W.: Flexural waves in a floating ice sheet: Modeling and comparison with data, The Journal of the Acoustical Society of America, 97, 971–977, https://doi.org/10.1121/1.412076, 1995.

Zhan, Z.: Distributed Acoustic Sensing Turns Fiber-Optic Cables into Sensitive Seismic Antennas, Seismological Research Letters, 91, 1–15, https://doi.org/10.1785/0220190112, 2019.

440 Zhou, Y., Yue, H., Kong, Q., and Zhou, S.: Hybrid Event Detection and Phase-Picking Algorithm Using Convolutional and
Recurrent Neural Networks, Seismological Research Letters, 90, 1079–1087, https://doi.org/10.1785/0220180319, 2019.

Zhu, W. and Beroza, G. C.: PhaseNet: a deep-neural-network-based seismic arrival-time picking method, Geophysical Journal
International, 216, 261–273, https://doi.org/10.1093/gji/ggy423, 2019.

445
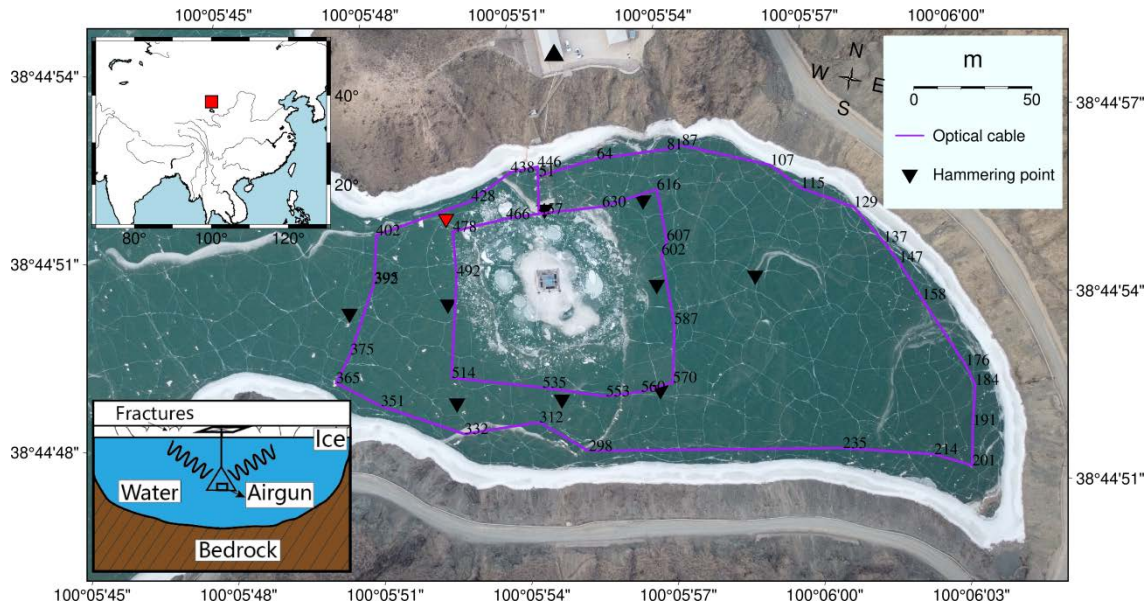
Figure 1: The experimental setting. The instrumented frozen lake is at Xiliushui Reservoir in Gansu Province, China (red rectangle in the inset). The optical fibre is marked with purple lines with channel number between 51-645 with gauge length of 10 m and a sampling rate of 1000 Hz. The airgun floating platform is at the centre of the lake. A reference broadband seismic station
450 **is marked with a triangle. Hammering points are marked with inverted triangles. The red triangle shows the one we use to measure the dispersion curve of flexural-gravity wave.**
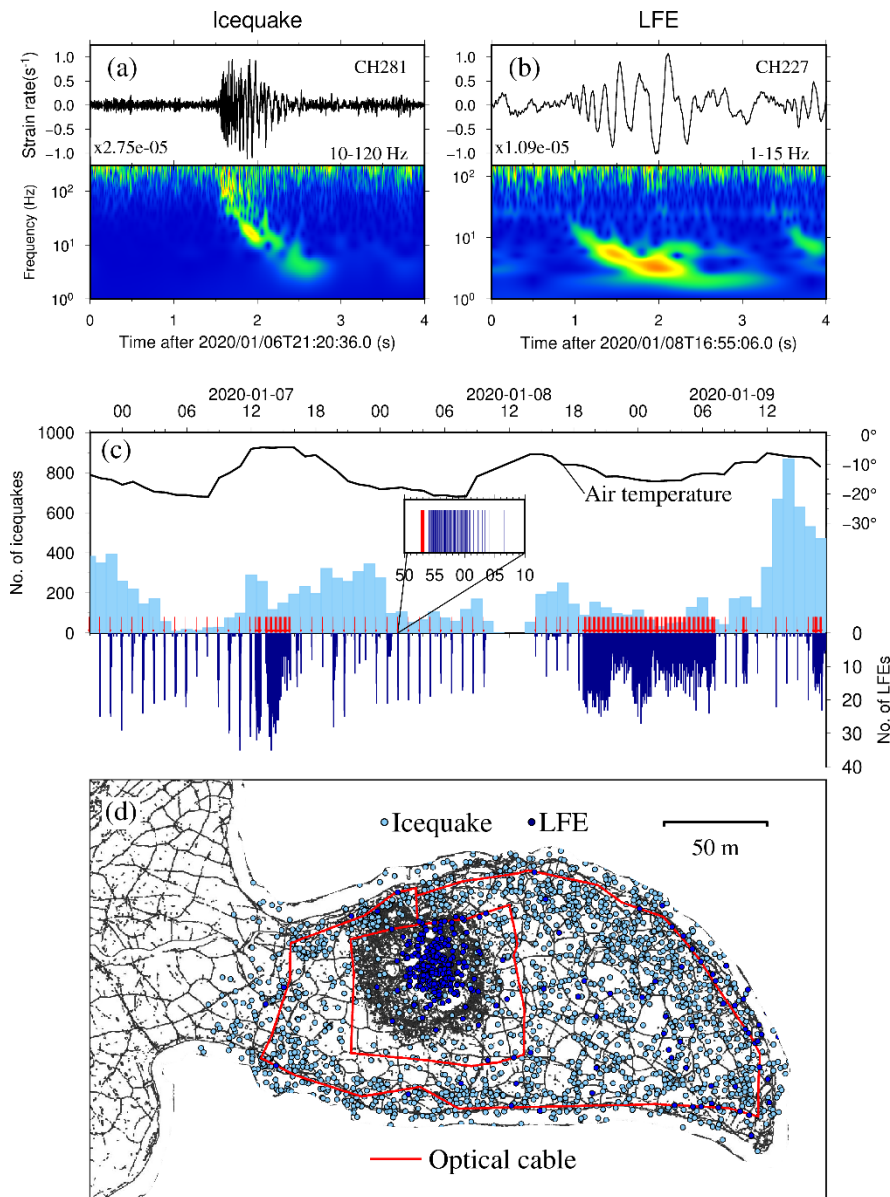
Figure 2: Typical passive signal waveforms, temporal and spatial distributions. (a) Icequake wave recorded by channel 281. The waveform is bandpass filtered in the frequency band of 10-120 Hz. (b) LFE waveform by channel 227. The waveform is bandpass filtered in the frequency band of 1-15 Hz. (c) temporal distributions for icequakes (light blue) per hour and LFEs (dark blue) per minute and the local air temperature (black curve). The temperature data is from European Centre for Medium-Range Weather Forecasts (https://www.ecmwf.int/). The time of AGE is marked with red arrow. The inset picture shows a window of 20 minutes with an AGE (red line) and following LFEs (black lines). The air temperature is denoted with black curve. (d) spatial distribution for icequakes (light blue) and LFEs (dark blue).
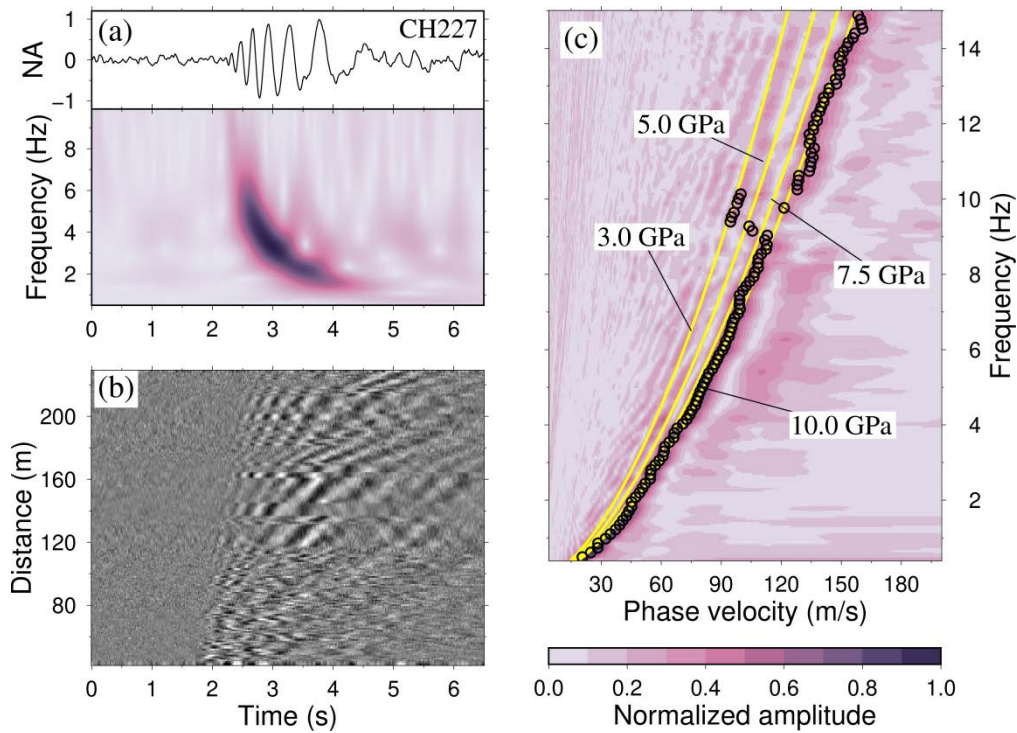
460

Figure 3: Dispersion analysis of LFEs. (a) Stacked LFE waveform and spectrogram of channel 227. The black curve is the stacked waveform with 272 LFE traces. It is bandpass filtered in the frequency band 1-15 Hz. The color denotes the normalized amplitude. (b) The record section of stacked waveform of all LFE events assuming all LFEs are originated at the AGE platform. (c) The measured phase velocity (circles) and predicted velocities (yellow curves) with different Young's modulus (3-10 GPa). The color

465   **means the dispersion spectra of stacked LFE traces in (c).**